Molecular dynamics comparative study of Lennard-Jones α-6 and exponential α-6 potentials: Application to real simple fluids (viscosity and pressure)

Guillaume Galliéro,[1,*] Christian Boned,[2] Antoine Baylaucq,[2] and François Montel[3]

[1]*Laboratoire d'Etude des Transfert d'Energie et de Matière, Université de Marne-la-Vallée,*

Bâtiment Lavoisier, Cité Descartes, Champs-sur-Marne, 77454 Marne-la-Vallée Cedex 2, France

[2]*Laboratoire des Fluides Complexes (UMR-5150), Université de Pau et des Pays de l'Adour,*

Boîte Postale 1155, 64013 Pau Cedex, France

[3]*TOTAL, CSTJF, Avenue Larribau, 64018 Pau, France*

In this work, using molecular dynamics simulation, the viscosity (dynamic property) and the pressure (static property) of spherical fluid particles interacting through Lennard-Jones α-6 and exponential α-6 potentials are computed. Simulations are performed for α going from 10 to 20 for the Lennard-Jones potential and from 12 to 22 for the exponential one. Six different thermodynamic states are tested that cover a large range of conditions, from sub- to supercritical temperature and from low to high density. To compare in a consistent manner the results for the various potentials tested, the simulations are carried out for the same set of reduced thermodynamic conditions (using the critical point). It is found that a perfect corresponding-states formulation is not possible between these potentials. Then, these potentials are applied on real simple fluids (argon, oxygen, nitrogen, methane, ethane, and one mixture, air) and the calculated viscosity and pressure values are compared with reference values. It appears that, using the appropriate α, both potential families lead to a good accuracy in pressure and viscosity using the same set of molecular parameters for both properties, the average absolute deviations being always lower than 5% for the studied states. In addition, it is shown that the exponential potential results do not outperform the Lennard-Jones ones. Furthermore, for all compounds except for methane, the best results are obtained for the Lennard-Jones 12-6 and the exponential 14-6 potentials. This result partly explains why, despite no theoretical background, the Lennard-Jones 12-6 potential is so widely used. Finally, it is shown that a van der Waals one-fluid model performs extremely well for the studied mixture (air).

I. INTRODUCTION

Among the intermolecular interaction potentials, the Lennard-Jones (LJ) 12-6 one is by far the most widely used in molecular simulations. Despite its simplicity, it has been shown to be able to exhibit most of the features experimentally found in fluid states. Furthermore, its formulation allows a relatively quick computation of the interaction in molecular dynamics (MD) simulations, which is a clear advantage compared to other interaction potentials. However, from a theoretical point of view, it is well-known [1] that the LJ 12-6 potential is not a true representation of even two-body interactions between argon atoms. It is an effective many-body empirical potential. The main weakness of the LJ 12-6 potential comes from the fact that it represents the decay of repulsive interaction by an inverse-12-power dependence on intermolecular separation whereas intermolecular repulsion decays exponentially. This point is of importance since it appears clearly that the structural properties of a normal fluid are primarily determined by the intermolecular short-range repulsive interactions [2,3].

An alternative to the classical two-parameter Lennard-Jones 12-6 potential, which can be correctly approximated by a short-range attractive potential [4], can be found in the more general three-parameter Lennard-Jones α-6 potential and in the three-parameter exponential α-6 (exp) potential family [5]. The last one uses an exponential formulation of the repulsive part of the potential. It is important to underline that up to now less attention has been paid to the exp potentials in molecular simulations. But recent simulations have shown the improved efficiency of the exp-6 potential over the LJ one for thermodynamic [6] and even for dynamic properties such as viscosity [7]. Concerning the influence of the repulsive part of the potential, it should be mentioned that some interesting results have been found recently for the purely repulsive soft sphere fluids [8], as well for the Lennard-Jones α-6 potential family [9].

Presently there is a demand for simple force fields to be able to accurately describe several properties simultaneously, which is not an easy task especially when static and dynamic properties are involved; see, for example, [10] for fluids modeled by a LJ 12-6 potential, [11] for molecular fluids modeled by inter- and intramolecular potentials, and [12] for polymer modeled by the LJ+freely jointed (FENE) approach. The first purpose of this paper is to compare the viscosity (dynamic property) and the pressure (static property) provided by molecular dynamics simulations on spherical fluid particles interacting through two types of force field, LJ and exp potentials, for various slopes of the repulsive part of the potential. The second purpose of this paper is to test the ability of the various potentials to reproduce, at the same time, the pressure and the viscosity of some simple real fluids in various thermodynamic states. To compare in a consistent manner the results for the various potentials tested,

———————
*Corresponding author. FAX: +33 1 60 95 72 94. Email address: galliero@univ-mlv.fr

TABLE I. Ratios r_{mij}/σ_{ij} for the various potentials.

α	10	12	14	16	18	20	22
LJ	1.13622	1.12246	1.11172	1.10305	1.09587	1.08980	
Exp		1.14122	1.12473	1.11284	1.103631	1.09619	1.09

the simulations have been carried out for the same set of reduced thermodynamics conditions (using the critical point as the scaling parameter).

Simulations are performed for α going from 10 to 20 for the LJ potential and from 12 to 22 for the exp one (which corresponds approximately to the same range of repulsive stiffness for both potentials). The six different states for which the simulations are performed for each potential cover a large range of thermodynamic conditions, from sub- to supercritical temperature and from low to high density. Then, results are applied on real simple compounds. The aim is to determine the relative efficiency of the LJ and of the exp potentials in modeling at the same time both viscosity and pressure of five simple fluids (argon, oxygen, nitrogen, methane, and ethane) and one mixture (air) with the same set of molecular parameters. Finally, the efficiency of a simple one-fluid approximation, the van der Waals one, is tested on the mixture studied (air).

II. THEORY

A. Fluid models

Interactions between a particle (i) and a particle (j) have been modeled using two families of effective potentials, the Lennard-Jones α-6 and the Buckingham or exponential α-6 ones, which can be written as [13]

$$U_{tot} = U_{repulsive} - \varepsilon_{ij}\left(\frac{\alpha_{ij}}{\alpha_{ij}-6}\right)\left(\frac{r_{m_{ij}}}{r_{ij}}\right)^6 \quad (1)$$

where for the Lennard-Jones potential

$$U_{repulsive} = \varepsilon_{ij}\left(\frac{6}{\alpha_{ij}-6}\right)\left(\frac{r_{m_{ij}}}{r_{ij}}\right)^{\alpha_{ij}} \quad (2)$$

and for the exponential-6 potential

$$U_{repulsive} = \varepsilon_{ij}\left(\frac{6}{\alpha_{ij}-6}\right)e^{-\alpha_{ij}(r_{ij}/r_{m_{ij}}-1)} \quad (3)$$

where ε_{ij} is the potential strength, r_{mij} the distance at which the potential is minimum, α_{ij} the stiffness of the repulsive slope, and r_{ij} the intermolecular separation. In this work α goes from 10 to 20 for the Lennard-Jones potential and from 12 to 22 for the exponential-6 one. It should be noted that the larger the repulsive exponent α_{ij}, the more repulsive the potential. For the same r_{mij}, the differences between the potentials for different α_{ij} are pronounced in the repulsive part of the potential (i.e., for $r_{ij} < r_{mij}$) but can be not negligible in the attractive part.

In the following, to define the dimensionless variables, the length σ_{ij} at which the potential is equal to zero ("the atomic diameter") has been used instead of r_{mij}. The ratios r_{mij}/σ_{ij} for all potentials tested are indicated in Table I. From this table, it appears that a LJ potential with a repulsive coefficient α is very similar to (i.e., has the same r_{mij} and a similar σ_{ij}) an exp potential with a repulsive coefficient $\alpha+2$.

B. Dimensionless and reduced variables

When using a spherical potential, it is convenient to use dimensionless variables, which are for the thermodynamic properties,

$$T^* = \frac{k_B T}{\varepsilon_x}, \quad \rho^* = \frac{N\sigma_x^3}{V}, \quad \text{and} \quad P^*(T^*,\rho^*) = P\frac{\sigma_x^3}{\varepsilon_x} \quad (4)$$

where T is the temperature, N the number of particles, V the volume of the simulation box, P the pressure of the system, and ε_x and σ_x the characteristic molecular parameters of the studied fluid (in pure fluids ε_x and σ_x are simply respectively equal to ε and σ of the fluid involved). It should be noted that the dimensionless pressure is a universal function, for a given potential form, of T^* and ρ^*.

In addition, a similar procedure can be achieved for transport properties [14,15]. The dimensionless viscosity, which is

TABLE II. Dimensionless critical parameters used to define the reduced T_r, ρ_r, and P_r for each potential.

α	10	12	14	16	18	20	22
T_c^*(LJ)	1.45	1.299	1.196	1.125	1.071	1.028	
ρ_c^*(LJ)	0.314	0.316	0.32	0.326	0.33	0.333	
P_c^*(LJ)	0.136	0.123	0.114	0.109	0.106	0.101	
T_c^*(exp)		1.404	1.253	1.157	1.088	1.039	1
ρ_c^*(exp)		0.314	0.321	0.326	0.327	0.329	0.332
P_c^*(exp)		0.132	0.120	0.112	0.105	0.102	0.098

TABLE III. Reduced thermodynamic states in which simulations have been performed.

	State 1	State 2	State 3	State 4	State 5	State 6
T_r	0.8	1	1	2	2	2
ρ_r	2.5	0.5	2	0.5	1	2

a unique function for a given potential form, is simply

$$\eta^*(T^*,\rho^*) = \eta \frac{\sigma_x^2}{\sqrt{m_x \varepsilon_x}} \qquad (5)$$

where m_x is the characteristic molecular weight of the fluid and η is the dynamic viscosity.

One may note that, when expressing a dynamic property in this set of dimensionless variables, the contributions of the thermodynamic state and of the molecular parameters are decoupled [16].

The critical point position, defined by the critical temperature T_c^* and the critical density ρ_c^*, is strongly dependent on the choice of the potential and its repulsive exponent. Therefore, to perform a consistent comparison between the results for different potentials, we have used the classical thermodynamic reduced conditions [15,16] which are, in this work, defined as

$$T_r = \frac{T^*}{T_c^*}, \quad \rho_r = \frac{\rho^*}{\rho_c^*}, \quad \text{and} \quad P_r = \frac{P^*}{P_c^*}. \qquad (6)$$

By using such scaling, and assuming it as adequate, i.e., a corresponding-states law, a given set of T_r and ρ_r will correspond to the same physical state (relatively to the critical point) whatever the potential and its repulsive coefficient. Indeed, if the reduced pressure is the same for two different potentials, then a corresponding-states approach is possible between the two potentials.

C. Nonequilibrium molecular dynamics

To compute the pressure and the viscosity, we have used a homemade code in FORTRAN 90. This code is based on the Verlet velocity algorithm to integrate the equation of motion. The usual periodic boundary conditions and minimum image convention were applied. In order to limit finite-size effects and to obtain a good accuracy on the value obtained, we have performed simulations on systems composed of 1500 particles. To ensure a sufficient statistical precision, we have performed simulations on 10^7 time steps. The dimensionless time step $t^* = (t/r_m)(\varepsilon/m)^{1/2}$ has been taken equal to 0.002. A truncated potential with a cutoff radius r_c equal to $2.5r_m$ has been used. A long-range correction for pressure was included in the computation.

Various algorithms are available to compute the viscosity through MD simulations [17], based on the equilibrium (EMD) or nonequilibrium [18] (NEMD) approach. Nonequilibrium approaches imply a perturbation of the system. Such perturbation may be used to study non-Newtonian viscosity or the thermodynamic behavior of fluids under shear [18–21], using the well-known SLLOD [18] algorithm, for example. With these techniques, if a sufficiently weak perturbation is applied, the classical dynamic viscosity may be extrapolated.

Among these nonequilibrium approaches, we have chosen to use a boundary-driven nonequilibrium scheme developed by Müller-Plathe [22], which provides reliable results in a reasonable amount of CPU time [23,24]. As indicated in [22], this NEMD approach is simple and keeps constant the overall energy and momentum of the system without any constraint on these quantities. A comparison of the results given by this scheme with more classical techniques (SLLOD and EMD) will be provided in the following section.

In this technique, the simulation box is divided in 32 slabs along the z direction. Then, the fluid is sheared using a net exchange of the momentum along the direction x (perpendicular to z), which is performed between the central part of the simulation box, slabs 16 and 17, and the edge layers, slab 1 and 32, to conserve the periodic boundary conditions. Hence, this scheme does not need a modification of the boundary conditions like for example the Lee-Edwards boundary conditions [18].

To perform the net exchange of momentum, we look for the two particles in slabs 1 and 32 with the largest negative x components of the momentum and for the two particles in slabs 16 and 17 with the largest positive x components of the momentum. Then, we exchange x components of the velocity between the particles involved. This procedure keeps constant the overall energy and momentum and corresponds to a redistribution in the simulation box of a certain amount of momentum [22]. This exchange is done every A time steps to avoid too large shear. After a transient stage, the system tends toward a stationary state and the viscosity of the system is simply deduced from the Newton's law. At the station-

TABLE IV. Dimensionless pressure for different Lennard-Jones potentials and for the six various states of the fluid.

State	LJ 10-6	LJ 12-6	LJ 14-6	LJ 16-6	LJ 18-6	LJ 20-6
1	1.156±0.015	1.042±0.012	1.022±0.01	1.054±0.011	1.084±0.013	1.053±0.012
2	0.129±0.003	0.114±0.002	0.107±0.002	0.102±0.002	0.099±0.001	0.096±0.002
3	0.543±0.005	0.485±0.004	0.472±0.005	0.488±0.006	0.486±0.004	0.475±0.004
4	0.436±0.003	0.393±0.004	0.376±0.003	0.358±0.003	0.348±0.004	0.339±0.003
5	0.931±0.007	0.849±0.005	0.812±0.007	0.797±0.006	0.782±0.007	0.767±0.007
6	3.516±0.025	3.343±0.022	3.317±0.019	3.392±0.023	3.419±0.029	3.424±0.017

TABLE V. Dimensionless pressure for different exponential potentials and for the six various states of the fluid.

State	Exp 12-6	Exp 14-6	Exp 16-6	Exp 18-6	Exp 20-6	Exp 22-6
1	1.104±0.010	1.176±0.014	1.166±0.012	1.011±0.012	0.933±0.01	0.907±0.009
2	0.122±0.002	0.111±0.003	0.103±0.002	0.097±0.003	0.094±0.002	0.091±0.002
3	0.503±0.006	0.506±0.004	0.491±0.007	0.432±0.007	0.420±0.005	0.412±0.005
4	0.416±0.004	0.385±0.003	0.364±0.005	0.346±0.004	0.335±0.004	0.327±0.005
5	0.881±0.007	0.833±0.007	0.801±0.006	0.767±0.007	0.748±0.005	0.736±0.005
6	3.261±0.031	3.323±0.023	3.347±0.029	3.257±0.027	3.232±0.019	3.246±0.025

ary state in the linear response regime, the shear rate is evaluated thanks to the local velocity computed in each slab.

The slabs where the exchanges are performed have been discarded to measure the shear rate. The exchange frequency needed in this algorithm has been taken equal to 300 to avoid any disturbances [24]. Such a large value of A induces a weak perturbation, and corresponds to a dimensionless shear rate always smaller than 0.005.

A simulation is composed of two steps: the first one consists in equilibrating the system to a desired temperature by imposing the temperature and the second one corresponds to the application of the NEMD scheme. In addition, as long as there is a transient state before the velocity gradient becomes stationary, the first 2×10^5 time steps of the NEMD simulations have been discarded for the measurement.

Using these numerical parameters, the statistical errors produced on viscosity are around +/−3%, except in dense phases where errors may reach 5%, and are around +/−1% on pressure.

It should be mentioned that such a scheme, with a sufficiently weak perturbation, does not warm up the system [22]. Nevertheless, as the duration of the simulations are important, to keep the temperature stable, we have used a Berendsen thermostat [25] with a large time constant $\tau_T = 1000t^*$.

D. Comparisons with previous literature results on molecular dynamics simulation

A test of the ability of our own code to provide consistent results on a LJ 12-6 pure fluid has been performed. First, the LJ viscosity has been evaluated at the classical state close to the triple point $T_{LJ}^* = 0.722$ and $\rho_{LJ}^* = 0.8442$. For this state, we have found a dimensionless viscosity η^* of 3.21 ± 0.11, which is consistent with the literature [26] (EMD and SLLOD algorithms).

Then, for different thermodynamic states, the results have been compared with those coming from a reliable study using equilibrium molecular dynamics on Lennard-Jones 12-6 particles [27]. Simulations have been performed at $T_{LJ}^* = 1$ and $\rho_{LJ}^* = 0.7$ and 0.9 and at $T_{LJ}^* = 2.5$ for ρ_{LJ}^* going from 0.3 to 0.9 with a step of 0.2.

To estimate the reliability of the N_c results, we have evaluated the average absolute deviation $\mathcal{D}_{AA}$

$$\mathcal{D}_{AA} = \frac{1}{N_c} \sum_{i=1}^{N_c} 100 \left| 1 - \frac{n_{this\ work}^*}{n_{Meier}^*} \right| \tag{7}$$

and the maximal deviation $\mathcal{D}_{Mx}$

$$\mathcal{D}_{Mx} = \max \left(100 \left| 1 - \frac{\eta_{this\ work}^*}{\eta_{Meier}^*} \right| \right) \tag{8}$$
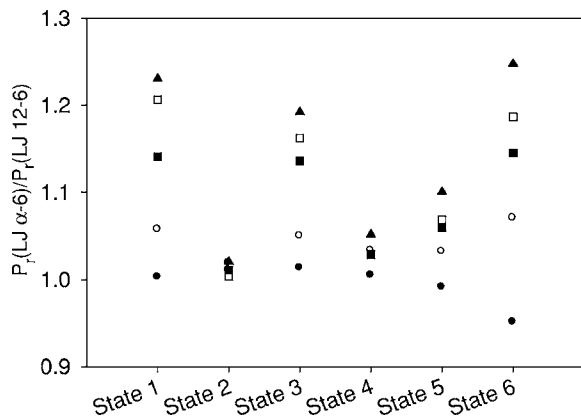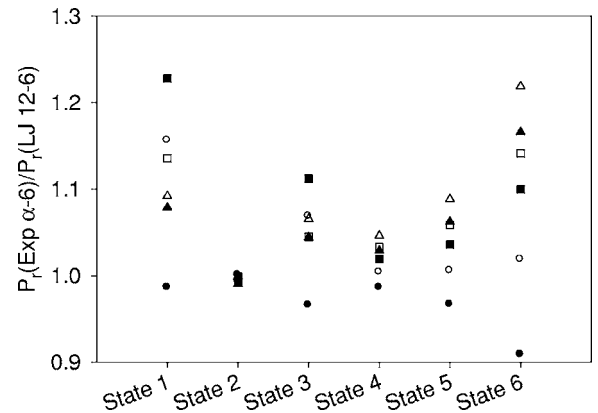

FIG. 1. Dependence on the state of the reduced pressure relative to the reduced pressure of the Lennard-Jones 12-6 potential, for the various Lennard-Jones α-6 potentials: α=(●)10, (○) 14, (■) 16, (□) 18, and (▲) 20.

FIG. 2. Dependence on the state of the reduced pressure relative to the reduced pressure of the Lennard-Jones 12-6 potential, for the various exponential α-6 potentials: α=(●) 12, (○) 14, (■) 16, (□) 18, (▲) 20, and (△) 22.

TABLE VI. Dimensionless viscosity for different Lennard-Jones potentials and for the six various states of the fluid.

State	LJ 10-6	LJ 12-6	LJ 14-6	LJ 16-6	LJ 18-6	LJ 20-6
1	1.778±0.064	1.927±0.094	2.096±0.082	2.371±0.096	2.611±0.112	2.861±0.101
2	0.210±0.004	0.193±0.005	0.182±0.004	0.173±0.005	0.172±0.005	0.166±0.004
3	0.882±0.024	0.896±0.019	0.959±0.031	0.996±0.027	1.046±0.025	1.071±0.031
4	0.345±0.007	0.329±0.008	0.302±0.006	0.285±0.009	0.289±0.006	0.279±0.006
5	0.452±0.012	0.424±0.011	0.427±0.009	0.427±0.012	0.419±0.013	0.413±0.01
6	0.965±0.025	1.013±0.031	1.083±0.017	1.139±0.029	1.194±0.027	1.231±0.029

which are both expressed as percentages.

For these six points, we have obtained $\mathcal{D}_{AA}$ of 1.64%, and a $\mathcal{D}_{Mx}$ of 3.48% [28]. It is worth noticing that the results are in good agreement despite the fact that the two techniques used are different, equilibrium and nonequilibrium methods, and that some parameters differ (e.g., Meier [27] uses a cutoff radius between 5σ and 6.5σ, and we use a cutoff radius equal to $2.5r_m$, i.e., about 2.8σ).

For the same six points, we have compared our results on pressure with the one provided by the equation of state of Kolafa and Nezbeda [29]. We have obtained an average absolute deviation of 0.69%, and a maximum deviation of 1.84%. The results are reasonably good compared to the inherent statistical errors of the simulations.

III. RESULTS

A. Methodology

Molecular dynamics results are mainly dependent on the choice of the fluid model, i.e., in our case the interaction potential. So simulations have been performed on the two families of potentials described by Eqs. (1)–(3). The idea is to evaluate their ability to simultaneously reproduce a static and a dynamic property, respectively, the pressure and the viscosity, of some simple real fluids.

For the LJ potential, α varies from 10 to 20 with a step of 2 and for the exp potential, α varies from 12 to 22 with a step of 2 (which corresponds to a similar range of repulsive slope for both potentials). This range of α for both potentials covers most of the usual values deduced in the low-density limit by the evolved kinetic theory for simple fluids [30]. Thus, 12 different potential shapes were tested.

In addition, to compare as accurately as possible the results for various potentials, we have performed simulations for the same sets of reduced thermodynamic conditions T_r and ρ_r [see Eq. (6)]. The critical dimensionless values T_c^* and ρ_c^* needed in Eq. (6) have been taken from [13], except for the LJ 10-6 which has been extrapolated from the values for $\alpha \geq 11$ using a polynomial form. They are summarized in Table II.

To cover a large range of thermodynamic states, without too many simulations, we have chosen six different characteristic states (see Table III), a liquid one (state 1), two on the critical isotherm (states 2 and 3), and three supercritical ones (states 4, 5, and 6).

B. Molecular dynamic simulation for both potential types

Dimensionless pressure results, Eq. (4), are given in Tables IV and V. To compare the results for both potentials and for the various repulsive exponents, the comparison should be done on the reduced pressure P_r defined by Eq. (6). As the most usual potential form is the Lennard-Jones 12-6 potential, the ratio between the reduced pressure for each potential and the reduced pressure for the Lennard-Jones 12-6 potential is presented (see Figs. 1 and 2).

Figures 1 and 2 show that the reduced pressures are strongly dependent on the repulsive exponent, as well as to the functional form of the repulsive part. In addition, the reduced pressure increases generally with the repulsive exponent, the effect being important in dense states (states 1, 3, and 6). Such results indicate that a perfect corresponding-states scheme is not possible between potentials of dissimilar repulsive exponents and different functional forms of the repulsive part. Nevertheless, for moderate and low densities, the discrepancies are not large. In addition, we can suspect that the behavior is slightly affected by the intrinsic imprecision of the critical values used.

The behavior of the dimensionless viscosity, Eq. (5), is given in Tables VI and VII. As long as the "critical" viscosity is not known (in fact the viscosity diverges close to the critical point), no direct comparison could be achieved through a reduced viscosity. Nevertheless, when looking at the dimensionless viscosity, it appears that for both potentials viscosity increases when repulsive slope increases for dense systems (states 1, 3, 6) and decreases slightly for low- and medium-density systems (states 2, 4, 5).

So the results for different potential forms and different repulsive exponents are not transferable from one to another through a corresponding-states scheme. This result is important as it implies that these various potentials will not be equivalent in representing real fluid values.

C. Application to real fluids

Once the results were obtained on the model fluids, we have tested the possibility of the various potentials to predict at the same time, with the same set of molecular parameters, both the pressure and the viscosity of real fluids. Such a comparison implies using an accurate equation of state (EOS) and a correlation on viscosity as precise as possible for each of the tested fluids. For each compound, the most recent correlation was chosen. In addition, this comparison
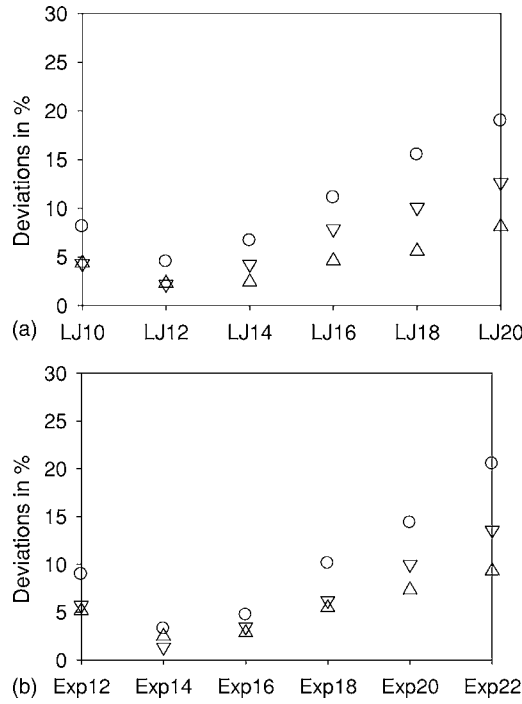
FIG. 3. Application of the LJ and exp results on viscosity and pressure for various α to argon: Circles represent $\mathcal{D}_{Mx}$, up triangles the $\mathcal{D}_{AA}$ on viscosity and down triangles the $\mathcal{D}_{AA}$ on pressure.
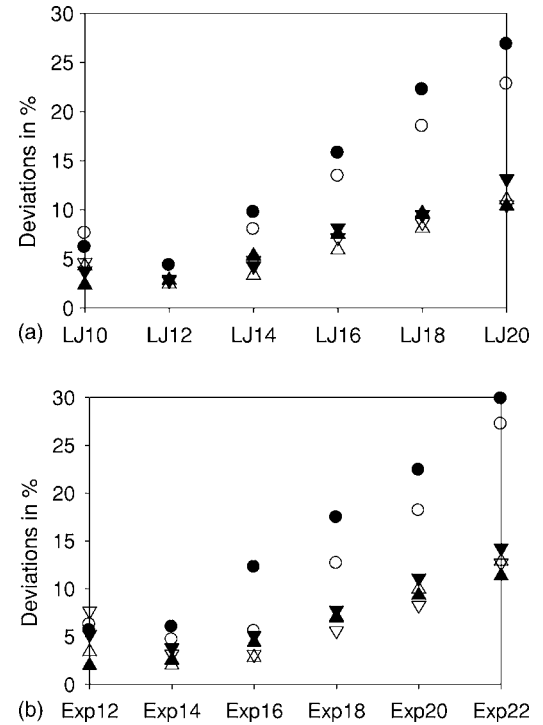

FIG. 4. Application of the LJ and exp results on viscosity and pressure for various α to oxygen (black symbols) and nitrogen (open symbols). Legend is the same as in Fig 3.

has been restricted to simple fluids (i.e., not polar, and not too aspherical) to keep a certain consistency.

The fluids tested are the following (EOS and correlation): methane [31,32], ethane [33], argon [34,35], oxygen [34,36], nitrogen [34,37], and air [34,38]. Notice that air is a mixture. The deviation on a quantity τ (representing P or η), is defined as

$$\mathcal{D}_{AA} = \frac{1}{6}\sum_{i=1}^{6} 100 \left| 1 - \frac{\tau_i^{MD}}{\tau_i^{corr}} \right| \qquad (9)$$

where the subscript i denotes the state, MD the results by molecular dynamic simulations, and $corr$, those coming from the EOS or the correlation on viscosity. The maximum absolute deviation $\mathcal{D}_{Mx}$ is defined as

$$\mathcal{D}_{Mx} = \max\left(100 \left| 1 - \frac{\tau_i^{MD}}{\tau_i^{corr}} \right| \right). \qquad (10)$$

For each potential and each compound, we have determined the set of molecular parameters (ε and σ) that minimize the

quantity $\mathcal{D}_{Mx}$ defined as half the sum of the $\mathcal{D}_{Mx}$ on viscosity and on pressure. In some sense we can consider that this set is the optimum set.

Results, in terms of $\mathcal{D}_{Mx}$ and $\mathcal{D}_{AA}$ are shown in Figs. 3–6. From these figures, it appears that the results provided by the LJ and exp potentials are very similar whatever the compound, thus no real improvement of results of the exp potential over the LJ one can be found. Therefore, for this range of thermodynamic states and for the studied properties, the choice of an exp potential is questionable (due to its CPU time needs compared to a LJ one).

In addition, it is interesting to note that, except for methane, a clear minimum appears for each compound (see Figs. 3–6). Furthermore, the best results are obtained for $\alpha=12$ for the LJ potential and for $\alpha=14$ for the exp one (except for methane). This result is interesting and important, because it partly explains why the LJ 12-6 potential is still so widely used, despite the lack of theoretical background of the repulsive coefficient (exponent 12). Concerning methane, Fig. 5

TABLE VII. Dimensionless viscosity for different exponential potentials and for the six various states of the fluid.

| State	Exp 12-6	Exp 14-6	Exp 16-6	Exp 18-6	Exp 20-6	Exp 22-6
1	1.764±0.085	2.082±0.062	2.335±0.095	2.428±0.081	2.559±0.079	2.864±0.105
2	0.199±0.004	0.187±0.005	0.179±0.004	0.169±0.005	0.165±0.004	0.162±0.004
3	0.862±0.019	0.941±0.027	0.996±0.021	1.011±0.019	1.033±0.024	1.067±0.026
4	0.333±0.006	0.306±0.007	0.296±0.005	0.284±0.006	0.272±0.005	0.275±0.005
5	0.442±0.009	0.418±0.012	0.415±0.014	0.413±0.011	0.406±0.017	0.406±0.012
6	0.932±0.031	1.006±0.019	1.069±0.022	1.111±0.024	1.150±0.028	1.226±0.032
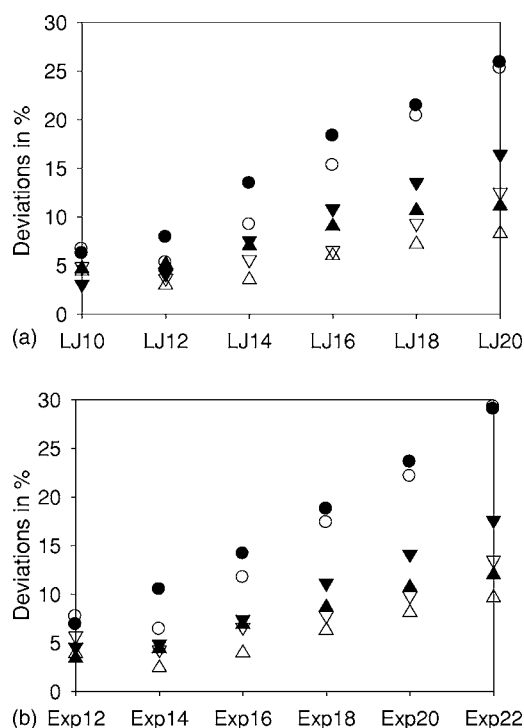
FIG. 5. Application of the LJ and exp results on viscosity and pressure for various α to methane (black symbols) and ethane (open symbols). Legend is the same as in Fig 3.

FIG. 6. Application of the LJ and exp results on viscosity and pressure for various α to air. Legend is the same as in Fig 3.

indicates that the best results are obtained for the lowest α for both potentials (i.e., 10 for the LJ potential and 12 for the exp one).

Another important point is that this approach clearly shows that, except for methane, with the same set of molecular parameters, pressure and viscosity of some simple pure compounds (spherical such as argon and even slightly aspherical such as ethane) can be correctly estimated using only the classical LJ 12-6 potential. Furthermore, it should be noted that, for air, which is a mixture mimicked by a single pseudocompound, results are remarkably good despite the simplicity of the approach.

Thus, using a LJ 12-6 potential, the $\mathcal{D}_{Mx}$ on both properties is generally smaller than 6%, which is excellent taking into account the different intrinsic errors and the diversity of fluid states tested. In addition, the $\mathcal{D}_{AA}$ on each property is always smaller than 5%. This is particularly interesting for mixtures, because the choice of a LJ 12-6 potential for all components avoids the need of any combining rule on the α parameters. Such a combination rule may cause the results to deteriorate in mixtures if the components are modeled by LJ α-6 or exp α-6 potentials with different α.

The optimum sets of molecular parameters deduced from this approach, for each compound tested, are given in Table VIII. It should be noted that the values are consistent with what is classically used in molecular simulations, despite differences (e.g., for Ar represented by a LJ 12-6, σ=3.405 Å and ε=996 kJ/mol in [39], which is very close to the values obtained here, σ=3.408 Å and ε=989 kJ/mol; see Table VIII, row LJ12).

In addition, concerning the air mixture, it is interesting to compare the set of molecular parameters given in Table VIII,
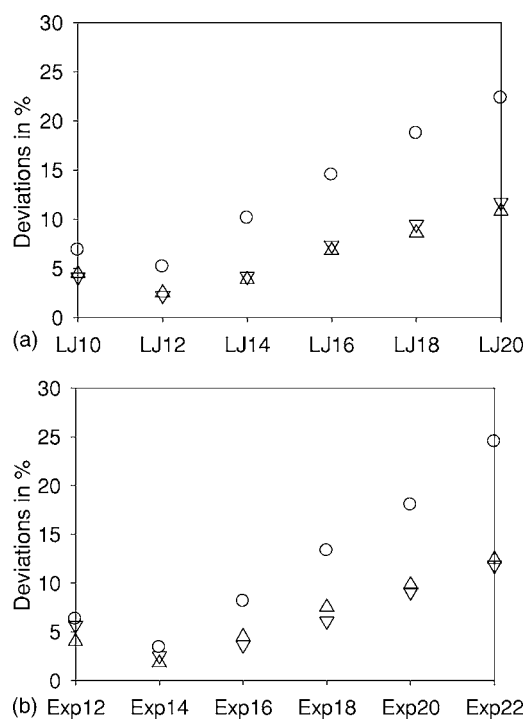
for a given potential, to those deduced from a one-fluid approximation [15]. This approach assumes that it is possible to lump the mixture compounds into a pseudocompound "equivalent" to the mixture. The molecular parameters of the pseudocompound are deduced from those of each compound and from a one-fluid model. We have used the classical van der Waals one-fluid approximation which is written, for an N-component mixture, as

$$m_x = \sum_{i=1}^{N} x_i m_i, \tag{11}$$

$$\sigma_x^3 = \sum_{i=1}^{N} \sum_{j=1}^{N} x_i x_j \sigma_{ij}^3, \tag{12}$$

$$\epsilon_x \sigma_x^3 = \sum_{i=1}^{N} \sum_{j=1}^{N} x_i x_j \epsilon_{ij} \sigma_{ij}^3, \tag{13}$$

where ε_x, σ_x, and m_x are the molecular parameters of the equivalent pseudocompound and x_i are the molar fractions.

As an example, this one-fluid approximation is applied to the Lennard-Jones 12-6 potential. This approach yields σ=3.562 Å and ε=854 kJ/mol (with a molar composition of 78.1% of N_2, 20.95% of O_2, and 0.95% of Ar), which is very close to what is directly found (ε=849.2 kJ/mol and σ=3.562 Å; see Table VIII, row LJ12). Using the molecular parameters deduced from the one-fluid model, we obtained for viscosity $\mathcal{D}_{AA}$=2.54% ($\mathcal{D}_{Mx}$=5.09%) and for pressure $\mathcal{D}_{AA}$=2.33% ($\mathcal{D}_{Mx}$=3.37%). This result indicates that for such simple mixtures this one-fluid model is efficient, which

TABLE VIII. Values of the optimum atomic diameter σ (in Å), and potential depth ε (in kJ/mol) for all potentials and compounds.

	Argon		Nitrogen		Oxygen		Methane		Ethane		Air	
	ε	σ	ε	σ	ε	σ	ε	σ	ε	σ	ε	σ
LJ10	906.6	3.415	745.4	3.617	914.4	3.384	1134.6	3.722	1781.7	4.237	777.3	3.567
LJ12	989.0	3.408	820.5	3.614	994.1	3.368	1212.6	3.704	1977.9	4.239	849.2	3.562
LJ14	1043.3	3.393	851.5	3.590	1061.7	3.364	1294.2	3.700	2125.5	4.228	904.0	3.546
LJ16	1092.6	3.395	903.6	3.596	1108.6	3.363	1358.6	3.704	2220.2	4.227	948.7	3.549
LJ18	1136.3	3.392	948.1	3.596	1164.5	3.360	1404.5	3.702	2310.7	4.223	987.0	3.547
LJ20	1170.2	3.394	986.7	3.600	1184.7	3.356	1440.0	3.701	2369.7	4.218	1019.1	3.549
Exp12	927.1	3.413	775.9	3.626	935.0	3.384	1150.3	3.727	1817.7	4.233	796.4	3.568
Exp14	1013.9	3.404	848.9	3.616	1023.6	3.365	1260.2	3.705	2038.6	4.234	877.6	3.563
Exp16	1082.4	3.400	882.6	3.600	1084.4	3.361	1323.6	3.702	2171.7	4.226	937.4	3.555
Exp18	1127.5	3.400	935.2	3.603	1132.9	3.362	1380.0	3.703	2265.7	4.226	977.0	3.554
Exp20	1160.3	3.400	977.2	3.607	1172.1	3.362	1432.5	3.705	2346.0	4.226	1011.1	3.555
Exp22	1184.3	3.397	1013.0	3.603	1200.4	3.357	1460.5	3.701	2403.1	4.220	1037.8	3.553

is consistent with previous observations [40] and could be valuable to provide values in simple mixtures (not too asymmetric ones).

IV. CONCLUSIONS

As previously mentioned in the Introduction, presently there is a demand for force fields to be able to accurately describe several properties at the same time, which is not an easy task especially when static and dynamic properties are simultaneously involved. In this work, using molecular dynamics simulation, the viscosity (dynamic property) and the pressure (static property) of spherical fluid particles interacting through either Lennard-Jones α-6 or exponential α-6 potentials have been computed. Notice that, up to now, less attention has been paid to the exp potentials in molecular simulations.

Simulations have been carried out for various repulsive slopes (α going from 10 to 20 for the Lennard-Jones potential and from 12 to 22 for the exponential one, both with a step of 2). Six different thermodynamic states have been tested that cover sub- to supercritical temperature and low to high density. The simulations have been performed for the same set of reduced thermodynamics conditions by using the critical temperature and density as references. Such procedure allows a consistent comparison of the results obtained for the various potentials.

It has been found that generally, for both potentials, the reduced pressure decreases when the repulsive coefficient decreases, the effect being more pronounced in dense states. In addition, the results show that no corresponding-states approach is possible between potentials having different repulsive exponents as well as different functional forms.

This study has been applied on real simple fluids (argon, oxygen, nitrogen, methane, and ethane) and one mixture (air). The results have been compared with the most accurate equations of states (for pressure) and correlations (for viscosity) available in the literature.

It appears that, whatever the compound, a good accuracy ($\mathcal{D}_{AA}$ lower than 5%) on pressure and viscosity using the same set of molecular parameters for both properties can be achieved for the studied states, by each potential family (LJ and exp ones). In addition, these results show that the exp potential does not yield strongly improved results compared to the Lennard-Jones one. Furthermore, except for methane, the best results are obtained for the Lennard-Jones 12-6 and the exponential 14-6 potentials. This important result may explain, why, despite no theoretical basis, the Lennard-Jones 12-6 is so widely used.

Finally, concerning mixture, it is shown that the usual van der Waals one-fluid model, applied on the LJ 12-6 potential, is able to perform extremely well, at least for simple mixtures like air.

[1] A. J. Stone, *The Theory of Intermolecular Forces* (Clarendon Press, Oxford, 1996).

[2] I. Nezbeda, Mol. Phys. **103**, 59 (2005).

[3] T. Young and H. C. Andersen, J. Phys. Chem. B **109**, 2985 (2005).

[4] S. Hess and M. Kröger, Phys. Rev. E **64**, 011201 (2001).

[5] R. A. Buckingham, Proc. R. Soc. London, Ser. A **168**, 264 (1938).

[6] J. R. Errington and A. Z. Panagiotopoulos, J. Phys. Chem. B **103**, 6314 (1999).

[7] H. Zhang and J. F. Ely, Fluid Phase Equilib. **217**, 111 (2004).

[8] D. M. Heyes and A. C. Branka, Phys. Chem. Chem. Phys. **7**, 1220 (2005).

[9] I. I. Adamenko, A. N. Grigoriev, and Y. I. Kuzovkov, J. Mol. Liq. **105**, 261 (2003).

[10] E. Ruckenstein and H. Liu, Ind. Eng. Chem. Res. **36**, 3927 (1997).

[11] M. G. Martin and A. P. Thomson, Fluid Phase Equilib. **217**, 105 (2004).

[12] M. Kröger, Phys. Rep. **390**, 453 (2004).

[13] A. Z. Panagiotopoulos, J. Chem. Phys. **112**, 7132 (2000).

[14] J. P. Boon and S. Yip, *Molecular Hydrodynamics* (Dover, New York, 1991).

[15] B. E. Poling, J. M. Prausnitz, and J. P. O'Connell, *The Properties of Gases and Liquids* (McGraw-Hill, New York, 2001).

[16] J. Vidal, *Thermodynamique: Application au Génie Chimique et à l'Industrie Pétrolière* (Technip, Paris, 1997).

[17] B. Hess, J. Chem. Phys. **116**, 209 (2002).

[18] D. J. Evans and G. Moriss, *Statistical Mechanics of Nonequilibrium Liquids* (Academic Press, London, 1990).

[19] J. Ge, G. Marcelli, B. D. Todd, and R. J. Sadus, Phys. Rev. E **64**, 021201 (2001).

[20] J. Ge, B. D. Todd, G. Wu, and R. J. Sadus, Phys. Rev. E **67**, 061201 (2003).

[21] G. Marcelli, B. D. Todd, and R. J. Sadus, Fluid Phase Equilib. **183-184**, 371 (2001).

[22] F. Müller-Plathe, Phys. Rev. E **59**, 4894 (1999).

[23] F. Muller-Plathe and D. Reith, Comput. Theor. Polym. Sci. **9**, 203 (1999).

[24] P. Bordat and F. Müller-Plathe, J. Chem. Phys. **116**, 3362 (2002).

[25] H. J. C Berendsen, J. P. M. Postma, W. F. van Gunsteren, A. di Nola, and J. R. Haak, J. Chem. Phys. **81**, 3684 (1984).

[26] K. Meier, Ph.D. thesis, University of the Federal Armed Forces, Hamburg, 2002 (unpublished).

[27] K. Meier, A. Laesecke, and S. Kabelac, J. Chem. Phys. **121**, 3671 (2004).

[28] G. Galliero, C. Boned, A. Baylaucq, and F. Montel, Fluid Phase Equilib. **234**, 56 (2005).

[29] J. Kolafa and I. Nezbeda, Fluid Phase Equilib. **100**, 1 (1994).

[30] S. Chapman and T. G. Cowling, *The Mathematical Theory of Non-Uniform Gases* (Cambridge Mathematical Library, Cambridge, 1990).

[31] E. Vogel, J. Wilhelm, C. Küchenmeister, and M. Jaeschke, High Temp. - High Press. **32**, 73 (2000).

[32] U. Setzmann and W. Wagner, J. Phys. Chem. Ref. Data **20**, 1061 (1991).

[33] D. G. Friend, G. Ingham, and J. F. Ely, J. Phys. Chem. Ref. Data **20**, 275 (1991).

[34] E. W. Lemmon and R. T. Jacobsen, Int. J. Thermophys. **25**, 21 (2004).

[35] Ch. Tegeler, R. Spanand, W. Wagner, J. Phys. Chem. Ref. Data **28**, 779 (1999).

[36] R. B. Stewart, R. T. Jacobsen, and W. Wagner, J. Phys. Chem. Ref. Data **20**, 917 (1991).

[37] R. Span, E. W. Lemmon, R. T. Jacobsen, W. Wagner, and A. J. Yokozeki, J. Phys. Chem. Ref. Data **29**, 1361 (2000).

[38] E. W. Lemmon, R. T. Jacobsen, S. G. Penoncello, and D. G. Friend, J. Phys. Chem. Ref. Data **29**, 331 (2000).

[39] P. Borgelt, C. Hoheisel, and G. Stell, Phys. Rev. A **42**, 789 (1990).

[40] G. Galliero, C. Boned, and A. Baylaucq, Ind. Eng. Chem. Res. **44**, 6963 (2005).